ALIN Framework (Adaptive Lethal Intersection Network): Pan-Cancer Generalization of Tri-Axial Combination Therapy to Prevent Drug Resistance

Roy Erzurumluoğlu*

Maastricht University, Bachelor of Natural Sciences, Maastricht, The Netherlands. Current affiliation: none.

February 6, 2026

Abstract

Cancer drug resistance arises when tumors shift signaling through compensatory pathways upon targeted inhibition. Liaki et al. [19] (PNAS 2025) demonstrated a solution in pancreatic cancer: simultaneously targeting three independent signaling axes—downstream, upstream, and orthogonal—prevents resistance because tumor cells survive through *any one* remaining active node.

We present ALIN Framework (Adaptive Lethal Intersection Network), a computational pipeline that generalizes this tri-axial inhibition principle to all DepMap cancer types. ALIN identifies cancer-specific viability paths, discovers which target combinations intersect every path via minimal hitting set optimization, and generates **ranked triple combinations** scored for tri-axial coverage, synergy, resistance prevention, toxicity, and druggability.

Across 96 cancer types, we generate predictions for **77 cancers** with **60.9% recall** against 23 gold-standard validated combinations (vs. 20.6% random, 39.1% top-genes baseline; $p < 0.001$). Key findings: (1) **STAT3** appears in 78% of predictions, confirming its role as the dominant orthogonal survival node across cancers; (2) a convergent tri-axial architecture emerges: STAT3 (orthogonal) + cell cycle regulators (downstream) + cancer-specific driver (upstream); (3) ODE-based pathway shifting simulation demonstrates that tri-axial combinations reduce tumor viability by **31.7%** compared to same-axis combinations across five cancers; (4) 88% of predictions include druggable targets. These results provide a systematic rationale for adding STAT3 inhibitors to existing targeted therapy trials across cancer types.

Keywords: cancer — drug resistance — tri-axial inhibition — combination therapy — DepMap — STAT3 — pathway shifting — precision oncology
Corresponding author: roy.erzurumluoglu@gmail.com

Introduction

Single-agent cancer therapies fail because tumors adapt: when one signaling pathway is inhibited, parallel or compensatory pathways sustain tumor cell survival. This *pathway shifting* is the fundamental mechanism of acquired drug resistance [3, 31]. Combination therapy addresses this by

*Corresponding author: roy.erzurumluoglu@gmail.com

simultaneously blocking multiple survival axes, but the vast combinatorial space (∼20,000 genes → millions of possible combinations) makes rational design essential.

Liaki et al. [19] recently demonstrated a powerful solution to drug resistance in pancreatic ductal adenocarcinoma (PDAC). They showed that PDAC tumor cells maintain viability through three independent signaling nodes: **downstream** (RAF1), **upstream** (EGFR), and **orthogonal** (STAT3) to KRAS signaling. Crucially, expression of *any single* node is sufficient to maintain tumor cell proliferation—ablating two nodes triggers compensatory activation of the third (e.g., RAF1+EGFR ablation activates STAT3 via FYN kinase phosphorylation [5, 4]). Only simultaneous targeting of all three axes—pharmacologically achieved with daraxonrasib (RAS inhibitor) [21], afatinib (EGFR/HER2 inhibitor) [15, 14], and SD-36 (STAT3 PROTAC) [1]—induced complete tumor regression with no resistance for >200 days. Dual combinations failed in all tested permutations [19].

This tri-axial inhibition principle provides a biologically principled framework for combination therapy design: to prevent pathway shifting, one must simultaneously block the downstream effector, the upstream activator, and the orthogonal survival node. However, generalizing this principle beyond PDAC requires answering a cancer-specific question: *which genes occupy the downstream, upstream, and orthogonal positions for each cancer type?*

We present ALIN Framework (Adaptive Lethal Intersection Network), a computational pipeline that addresses this question systematically. ALIN infers cancer-specific viability paths (functional survival mechanisms from DepMap + OmniPath data), then identifies target combinations that cover every viability axis. The **minimal hitting set (MHS)** [30, 22] formalizes target selection as a combinatorial optimization problem, while **ranked triple combinations** scored for pathway diversity (tri-axial coverage), synergy, resistance prevention, and toxicity provide clinically actionable predictions.

Our contributions: (1) pan-cancer generalization of the tri-axial principle to 77 cancer types; (2) identification of convergent target architecture across cancers; (3) ranked triple combinations with multi-source validation; (4) benchmarking against 23 clinically validated combinations (60.9% recall); (5) ODE-based simulation demonstrating 31.7% viability advantage of tri-axial over same-axis combinations.

Methods

Data sources

We use DepMap [9, 28] release 24Q4 (accessed January 2025) for gene dependency $D_{g,\ell}$ (Chronos score [9] from CRISPRGeneEffect.csv), cell line metadata (Model.csv), and cancer type mapping via OncoTree (OncotreePrimaryDisease). OmniPath [29] provides the directed signaling network $G = (V, E)$ (accessed January 2025; cached for reproducibility). PRISM [7] and GDSC [32, 16] supply drug sensitivity data for validation. All data versions and access dates are documented in VERSION_INFO.md in the code repository.

Viability path inference

Viability paths represent independent survival mechanisms that must each be blocked to prevent pathway shifting and resistance [19]. The Liaki et al. [19] finding that PDAC cells survive through *any one* of three signaling axes (RAF1, EGFR, STAT3) motivates our approach: we infer multiple distinct viability paths per cancer, then seek combinations that cover all of them. We infer paths

by four complementary approaches: co-essentiality clustering, signaling topology, cancer-specific statistical testing, and perturbation-response signatures.

1. Essentiality and selectivity. A gene is considered essential if its DepMap Chronos score is below -0.5 (standard threshold for essentiality [9, 2]). We retain only *selective* genes (those essential in $\geq$30% of cell lines for that cancer type) to filter noise from rare line-specific hits [26]. Pan-essential genes (essential in >90% of all cell lines across cancers—also termed housekeeping genes [10, 13]) are excluded to prioritize cancer-selective targets.

2. Co-essentiality clustering. Genes essential in the same cell lines often belong to the same pathway [23]. We compute co-essentiality as the fraction of cell lines where both genes are essential, then apply hierarchical clustering to group co-essential genes into 3–15 viability modules. This captures functional relationships without requiring prior pathway knowledge.

3. Signaling paths. Co-essentiality captures modules but not directionality. We therefore extract paths from the OmniPath directed network [29] connecting driver genes (KRAS, BRAF, EGFR) to essential effectors (CDK4, STAT3, BCL2). Paths are limited to 4 hops (typical signaling depth) and scored by mean dependency of constituent genes. Paths with weakly essential genes are pruned.

4. Cancer-specific dependencies. Genes significantly more essential in the target cancer than in other cancers (Welch t-test, FDR-corrected $q < 0.05$, Cohen's $d > 0.3$ [6]) form an additional path. This captures lineage-specific vulnerabilities not evident from co-essentiality or topology alone. The Cohen's $d > 0.3$ threshold represents a small-to-medium effect size [6], providing a conservative cutoff balancing sensitivity and specificity.

5. Perturbation-response paths. Methods 1–4 rely on baseline co-essentiality and static network topology, missing dynamic pathway relationships revealed by perturbation. We incorporate curated phosphoproteomics and transcriptional response signatures from published inhibitor studies: when KRAS is inhibited, ERK/RSK phosphorylation decreases while EGFR/MET phosphorylation increases (feedback reactivation); when CDK4/6 is inhibited, RB1/E2F targets decrease while CDK2/CCNE1 increase (bypass). Essential genes that overlap with these perturbation responders form additional viability paths. The feedback/reactivation genes (e.g., EGFR after KRAS inhibition, CDK2 after CDK4 inhibition) inform resistance scoring: combinations that also target feedback genes receive a bonus. This approach captures functional pathway membership validated by experimental perturbation rather than inferred from co-occurrence or network proximity.

Full mathematical definitions are provided in the code repository (`METHODOLOGY_JUSTIFICATION.md`).

Minimal hitting set (MHS) optimization

We frame target selection as a **minimal hitting set** problem [30, 22]: find a minimal set of genes T that intersects every viability path. This provides a theoretical lower bound on the number of targets needed for complete path coverage. However, by design, minimal hitting sets optimize for parsimony—they find the *fewest* targets, not necessarily targets from three independent signaling axes. The Liaki et al. [19] results demonstrate that even when two targets might cover all static paths, the tumor can dynamically activate a third pathway upon treatment. Therefore, we treat the MHS as a **computational foundation** and generate ranked triple combinations (below) as the primary therapeutic recommendation. The core constraint is:

$$\forall p \in P: \quad T \cap \mathcal{N}(p) \neq \emptyset \tag{1}$$

where P is the set of viability paths and $\mathcal{N}(p)$ denotes genes in path p.

We minimize a **weighted cost** that penalizes toxic and pan-essential genes while rewarding tumor-specific and druggable targets:

$$c(g,c) = \underbrace{\tau(g)}_{\text{toxicity}} - 0.5 \cdot \underbrace{s(g,c)}_{\text{specificity}} - 0.3 \cdot \underbrace{d(g)}_{\text{druggability}} + 2 \cdot \underbrace{\mathbb{1}_{\text{pan}}}_{\text{penalty}} + 1 \tag{2}$$

Toxicity scores derive from DrugTargetDB and OpenTargets safety data. Tumor specificity measures how much more essential a gene is in this cancer versus all cancers (higher = more specific). Druggability reflects whether approved drugs exist (1.0) or the target is preclinical (0.2).

Solvers. We use greedy selection (iteratively adding the gene with best coverage-per-cost ratio) for speed, and exhaustive enumeration for small candidate sets ($\leq$25 genes) to guarantee optimality. The algorithm does not fix the combination size *a priori*—the optimal number of targets (1–4 in practice) emerges from the cancer's viability network complexity.

Ranked triple combination scoring

For clinical translation and benchmarking, we additionally enumerate **triples** (three-target combinations, matching the Liaki et al. [19] triple-therapy design) from the candidate gene pool and score each by five criteria:

Path coverage: fraction of viability paths hit by the triple (minimum 70% required).

Synergy score: combines known synergistic pairs from clinical data (e.g., BRAF+MEK, KRAS+STAT3) with pathway diversity. Triples hitting three distinct pathways (e.g., cell cycle + MAPK + JAK/STAT) score higher than triples hitting one pathway three times.

Resistance probability: estimates likelihood of bypass resistance using curated resistance mechanisms (e.g., EGFR inhibitor resistance via MET amplification [3, 31]). Triples that also target known bypass genes score lower (better).

Combination toxicity (combo-tox): while per-target toxicity addresses single-drug safety, combination therapy introduces additional risks from drug-drug interactions and overlapping toxicities. We incorporate three complementary signals: (1) *Known DDIs*: curated contraindications from clinical literature (e.g., QT prolongation with trametinib+dasatinib, additive myelosuppression with palbociclib+venetoclax); (2) *Overlapping toxicity classes*: when multiple drugs in a triple share the same toxicity profile (e.g., both cause neutropenia), the additive risk is penalized; (3) *FAERS co-adverse event signals*: elevated serious adverse event rates for drug pairs co-administered in FDA FAERS/MedWatch reports. Major DDIs contribute 0.4 to the combo-tox score, moderate DDIs 0.2, and overlapping toxicities 0.08–0.15 per shared class depending on severity. This approach captures combination-specific risks that per-target scoring misses.

Druggability: counts how many targets have FDA-approved drugs available.

These components are combined into a single ranking score:

$$\boxed{\begin{aligned} S_{\text{comb}} = {} & 0.22 \cdot \text{cost} + 0.18 \cdot (1 - \text{synergy}) + 0.18 \cdot \text{resistance} \\ & + 0.18 \cdot \text{combo-tox} + 0.14 \cdot (1 - \text{coverage}) \\ & - 0.10 \cdot n_{\text{drugs}} - \beta_{\text{pert}} \end{aligned}} \tag{3}$$

Lower scores indicate better combinations. The perturbation bonus β_{pert} rewards combinations that target feedback/bypass genes identified through perturbation-response signatures. Weights were validated by sensitivity analysis: perturbing weights $\pm$20% changed top-5 rankings in $<$15% of cancer types. Detailed scoring formulas are provided in the code repository.

Sensitivity and robustness

We assessed robustness to key parameters. Varying $\theta \in \{0.2, 0.3, 0.4\}$ (selectivity) and $\tau_{\text{dep}} \in \{-0.4, -0.5, -0.6\}$ (essentiality threshold), MHS compositions for major cancers (NSCLC, Colorectal, Breast, Melanoma, Pancreatic) remained stable: STAT3 and cell cycle regulators dominated across parameter settings. Varying combined-score weights ±20%, rank order of top 5 triples per cancer changed in $< 15\%$ of cases. Benchmark recall (60.9%) was robust to θ and τ_{dep} within tested ranges. Cancers with few cell lines ($n < 5$) showed higher variance in predicted MHS sets.

Validation and benchmarking

Validation: PubMed (literature co-mention), STRING (PPI, enrichment), ClinicalTrials.gov (trial matching), PRISM [7] (gene–drug correlation). Patient stratification: mutation-based subgroups (KRAS G12C, BRAF V600E), companion diagnostics. Benchmark: 23 gold-standard combinations; MHS sets are evaluated for superset matches; additionally, ranked triple combinations are generated and evaluated separately. Recall $= N_{\text{match}}/23$ where $N_{\text{match}} = |\{G : G \subseteq T \text{ for some predicted set } T\}|$. For single-drug entries targeting multiple proteins (e.g., palbociclib targets both CDK4 and CDK6), a match requires any one target protein to be present in the predicted set, reflecting drug-level equivalence. Baselines: random sampling (30 trials), top-genes (most frequent in DepMap).

Systems biology simulation: intra-axial MHS vs. tri-axial therapy

To quantify the impact of compensatory pathway shifting—the central biological argument for tri-axial inhibition—we developed an ODE-based systems biology model that explicitly simulates adaptive signaling dynamics under different treatment strategies. This addresses a key limitation of static essentiality data (DepMap CRISPR screens), which capture steady-state single-gene dependencies but not the dynamic pathway rewiring that occurs upon pharmacological multi-target inhibition.

Network construction. For five cancer types (PDAC, Melanoma, NSCLC, CRC, Breast), we constructed cancer-specific signaling networks comprising 10–14 nodes and 12–19 interactions, annotated with three biological axes: *upstream* drivers (constitutively active oncogenes: KRAS, BRAF, EGFR), *downstream* effectors (cascade nodes: RAF1, MEK, ERK, CCND1, CDK4), and *orthogonal* survival nodes (STAT3, FYN, MCL1, JAK family). Parameters were assigned based on biological role: constitutively active oncogenes received high basal production rates ($b = 0.25$–0.50), reflecting their mutational activation; cascade nodes received low basal rates ($b = 0.03$–0.08), making them depend on upstream input; orthogonal nodes received moderate basal rates ($b = 0.05$–0.10) with elevated compensatory gains ($g = 0.4$–0.7), reflecting their capacity for adaptive upregulation.

ODE model. Each node i follows:

$$\frac{dA_i}{dt} = \underbrace{\left[b_i + \textstyle\sum_j w_{ji} \cdot H(A_j)\right]}_{\text{production}} \cdot \underbrace{(1 - \delta_i(t))}_{\text{drug}} + \underbrace{C_i(\Delta_{\text{axes}})}_{\text{compensation}} - \underbrace{d_i \cdot A_i}_{\text{degradation}} - \underbrace{I_i}_{\text{inhibition}} \tag{4}$$

where $H(x) = x^2/(K^2 + x^2)$ is a Hill function [11] (half-max $K = 0.5$, coefficient $n = 2$), $\delta_i(t) = s_i(1 - e^{-\alpha t})$ is the time-dependent drug inhibition with strength $s_i = 0.92$ and onset rate $\alpha = 0.15\,\text{h}^{-1}$, and I_i captures network-level negative feedback (e.g., ERK⊣EGFR). The drug effect is *multiplicative* on production, modeling kinase inhibitors and PROTACs that reduce effective signaling output.

Compensatory pathway shifting. The compensation term C_i captures the Liaki de-repression mechanism: when drug treatment depletes axes *other* than node i's axis, uninhibited compensatory sources (e.g., FYN) activate orthogonal survival nodes (e.g., STAT3):

$$C_i = g_i \cdot \max\big(0, \bar{\Delta}_{\neg \text{axis}(i)} - 0.1\big) + \sum_{k \in \text{comp}(i)} w_{ki}^{(\text{comp})} \cdot H(A_k) \cdot \mathbb{1}[k \notin \mathcal{T}] \tag{5}$$

where $\bar{\Delta}_{\neg \text{axis}(i)}$ is the mean fractional activity loss in axes other than node i's own axis (relative to untreated homeostasis), and $\mathbb{1}[k \notin \mathcal{T}]$ ensures that compensation from a node k is suppressed if k itself is drug-inhibited. This captures the key biological insight: tri-axial combinations eliminate both direct activity *and* compensatory sources, while intra-axial MHS combinations leave orthogonal compensators intact.

Tumor viability. Following the Liaki principle that a tumor survives if *any* axis maintains sufficient activity:

$$V(t) = 0.6 \cdot \max_{\text{axis}} \bar{A}_{\text{axis}}(t) + 0.4 \cdot \text{mean}_{\text{axis}} \bar{A}_{\text{axis}}(t) \tag{6}$$

where $\bar{A}_{\text{axis}}$ is the mean activity of nodes in each axis.

Treatment strategies. We compared four strategies per cancer: (1) *no treatment*, (2) *single agent* (one upstream driver), (3) *MHS* (computationally-derived 2-target minimal hitting set, targeting nodes within the same cascade or axis), and (4) *tri-axial combination* (one target per biological axis: upstream + downstream + orthogonal). Simulations ran for 4800 h (200 days, matching the Liaki et al. [19] observation window) using RK45 integration (`scipy.integrate.solve_ivp`).

Results

Pan-cancer MHS discovery

We analyzed **96 cancer types** from DepMap (OncoTree primary disease mapping), spanning solid tumors, hematologic malignancies, and rare cancers; **77 cancer types** yielded MHS combinations (19 had insufficient cell lines or no viability paths). table 1 summarizes key metrics. A central finding is that the optimal MHS size varies by cancer: 11 cancers require only **1 target** (e.g., Chondrosarcoma: MCL1; Mucosal Melanoma: CCND1), 50 cancers require **2 targets**, 14 cancers require **3 targets**, and 2 cancers require **4 targets** (Colorectal Adenocarcinoma: CDK4+CTNNB1+KRAS+STAT3; Pleural Mesothelioma: CCND1+FGFR1+MDM2+STAT3). All 77 MHS sets achieve **100% viability path coverage**, meaning every inferred tumor survival mechanism is intersected.

Cell line counts per cancer type ranged from 1 (Ovarian Germ Cell Tumor, Glassy Cell Carcinoma) to 165 (Non-Small Cell Lung Cancer). Viability paths ranged from 4 (Chondrosarcoma, Mucosal Melanoma) to 103 (NSCLC), reflecting differences in tumor complexity. Cost scores ranged from 0.90 (Mixed Cervical Carcinoma, single ERBB2 target) to 4.57 (Pleural Mesothelioma, 4-target set).

Target frequency architecture

The most significant finding is the target frequency distribution across cancers (fig. 3):

- **STAT3** (60 cancers, 78%): The single most frequent MHS target, appearing across solid tumors, hematologic malignancies, and rare cancers. STAT3 is constitutively activated in >70% of solid tumors, promoting survival, immune evasion, and stemness downstream of multiple oncogenic drivers.

Table 1: Summary of pan-cancer MHS discovery metrics.

Metric	Value
Cancer types analyzed	96
Cancer types with MHS predictions	77
1-target MHS	11
2-target MHS	50
3-target MHS	14
4-target MHS	2
Viability path coverage (all)	100%
STAT3 frequency (of 77 cancers)	78% (60)
CCND1 frequency	23% (18)
MCL1 frequency	13% (10)
CDK4 frequency	10% (8)
CDK6 frequency	8% (6)
Benchmark recall (ranked triples)	60.9% (14/23)

- **CCND1** (Cyclin D1, 18 cancers, 23%): The second most frequent target, present in NSCLC, Melanoma, Pancreatic Adenocarcinoma, Renal Cell Carcinoma, Neuroblastoma, Liposarcoma, Ocular Melanoma, and others. CCND1 amplification drives G1/S transition and is targetable via CDK4/6 inhibitors (palbociclib, ribociclib) [27]. Its emergence as a high-frequency MHS reveals a pan-cancer cell cycle entry dependence distinct from CDK4/6 themselves.

- **MCL1** (10 cancers, 13%): An anti-apoptotic BCL-2 family member, appearing in NSCLC, Mature B-Cell Neoplasms, B-Cell ALL, Cervical SCC, Chondrosarcoma, and other cancers. MCL1 inhibitors (AMG-176, S64315) are in Phase 1 trials, positioning MCL1 as an emerging therapeutic target.

- **CDK4** (8 cancers, 10%) and **CDK6** (6 cancers, 8%): Cell cycle kinases with FDA-approved inhibitors, appearing in well-powered cancer types (Breast, Colorectal, Diffuse Glioma, AML, Ewing Sarcoma, Myeloproliferative Neoplasms).

- **EGFR** (3 cancers), **KRAS** (2 cancers), **BRAF** (1 cancer): Surprisingly rare as MHS components despite their oncogenic driver roles, because they are captured through viability paths rather than as direct hitting set members in most cancer types.

Tri-axial interpretation. The target frequency distribution maps directly onto the tri-axial principle of Liaki et al. [19]:

- **Orthogonal axis**: STAT3 (78% of cancers). Like STAT3 in PDAC, this node is activated through parallel kinases (FYN, SRC, JAK family) and cannot be eliminated by targeting the primary oncogenic driver alone. Its high frequency confirms that most cancers possess an orthogonal survival axis that must be explicitly addressed.

- **Downstream effector axis**: CCND1, CDK4, CDK6, CDK2 (collectively present in 42 cancers). These cell cycle regulators function as convergent downstream effectors of multiple oncogenic signaling pathways (RAS/MAPK, PI3K/AKT, WNT), analogous to the RAF1 node in the Liaki PDAC model.

- **Upstream driver axis**: KRAS, BRAF, EGFR, FGFR1, FLI1 (cancer-specific). These mutation-driven oncogenes provide the cancer-specific upstream signal, analogous to EGFR in the Liaki model. Their lower frequency as MHS components reflects the hitting set's preference for hub nodes; however, ranked triple scoring (below) recovers cancer-specific drivers as essential combination partners.

This convergent architecture—orthogonal survival hub + downstream cell cycle effector + cancer-specific upstream driver—generalizes the Liaki tri-axial principle across cancer types. The consistency of this pattern provides evidence that tri-axial inhibition may be a broadly applicable therapeutic strategy, not specific to PDAC.

Cancer-specific MHS predictions

Notable cancer-type-specific MHS predictions with their actual pipeline outputs:

- **Non-Small Cell Lung Cancer** (165 lines, 103 paths): **CCND1 + CDK2 + MCL1**. Cost: 4.15. Drugs: dinaciclib (CDK2, phase 2), AMG-176/S64315 (MCL1, phase 1). Driver landscape: TP53 LoF 83.7%, CDKN2A LoF 54.1%, KRAS 36.7% (G12C: 13.3%), EGFR 6.1%. This combination targets cell cycle (CDK2), cell cycle entry (CCND1), and anti-apoptosis (MCL1)—three functionally distinct survival mechanisms.

- **Melanoma** (135 lines, 73 paths): **BRAF + CCND1 + STAT3**. Cost: 2.96. Drugs: vemurafenib/dabrafenib (BRAF, approved), napabucasin (STAT3, phase 2). Driver landscape: CDKN2A LoF 71.6%, BRAF V600E 68.7%, TP53 LoF 25.4%. This extends BRAF inhibition with STAT3 and CCND1, addressing JAK/STAT-mediated resistance.

- **Colorectal Adenocarcinoma** (96 lines, 69 paths): **CDK4 + CTNNB1 + KRAS + STAT3** (4-target). Cost: 3.96. The only common solid cancer requiring 4 targets, reflecting the convergence of WNT (CTNNB1), MAPK (KRAS), JAK/STAT (STAT3), and cell cycle (CDK4) pathways in CRC biology. Driver landscape: TP53 LoF 71.4%, KRAS 46.0%, PIK3CA 20.6%, BRAF V600E 17.5%.

- **Pancreatic Adenocarcinoma** (64 lines, 50 paths): **CCND1 + KRAS** (2-target MHS). Cost: 1.94. The minimal hitting set identifies only 2 targets because KRAS is near-universally essential (93.5% mutation rate, 89.1% at G12). However, Liaki et al. [19] demonstrated that KRAS inhibition alone (or even KRAS + EGFR) is insufficient—STAT3 activates via FYN kinase as a resistance mechanism. This divergence highlights the difference between *static path coverage* and *dynamic pathway shifting*: DepMap single-gene knockouts do not capture the adaptive STAT3 activation that occurs upon RAS pathway inhibition. For PDAC, the ranked triple (KRAS + cell cycle + STAT3) should be preferred over the minimal 2-target MHS (see Discussion).

- **Diffuse Glioma** (96 lines, 77 paths): **CDK6 + CHMP4B + STAT3**. Cost: 3.34. Combines cell cycle (CDK6), ESCRT-III endosomal sorting (CHMP4B), and JAK/STAT (STAT3).

- **Acute Myeloid Leukemia** (64 lines, 34 paths): **CDK6 + DNM2 + STAT3**. Cost: 2.89. Targets cell cycle (CDK6), dynamin-mediated endocytosis (DNM2), and JAK/STAT (STAT3) in hematologic malignancy.

- **Ewing Sarcoma** (51 lines, 33 paths): **CDK4 + FLI1 + STAT3**. Cost: 2.71. Uniquely, this includes the EWS-FLI1 fusion gene product as an MHS target, validating the pipeline's ability to identify cancer-defining dependencies.

- **Pleural Mesothelioma** (36 lines, 27 paths): **CCND1 + FGFR1 + MDM2 + STAT3** (4-target). Cost: 4.57. The most complex MHS, reflecting mesothelioma's multiple survival axes: FGFR signaling, p53/MDM2, JAK/STAT, and cell cycle.

- **Chondrosarcoma** (9 lines, 4 paths): **MCL1** (single target). Cost: 0.96. The simplest MHS, suggesting that MCL1 inhibition alone may collapse all viability paths in this chemotherapy-resistant tumor.

- **Myeloproliferative Neoplasms** (18 lines, 16 paths): **ABL1 + CDK4 + STAT3**. Cost: 3.10. Includes ABL1, the target of imatinib—validating a known therapeutic dependency in myeloproliferative disease.

Ranked triple combinations: tri-axial therapeutic predictions

In addition to MHS discovery, we generate **ranked triple combinations** as the primary therapeutic recommendation for each cancer type. While the MHS identifies the minimal targets for static path coverage, ranked triples explicitly enforce **tri-axial diversity** through the pathway diversity score (weight 0.6 in the synergy scoring function), ensuring that each triple spans distinct functional categories—mirroring the downstream/upstream/orthogonal architecture validated by Liaki et al. [19].

Benchmarking ranked triples against 23 gold-standard combinations (fig. 4) yields **60.9% recall** (13 superset matches + 1 pairwise match = 14 total matches), mean rank 1.0 when matched. Random baseline: 20.6% ± 5.5% (30 trials). Top-genes baseline: 39.1%. ALIN significantly outperforms both baselines ($p < 0.001$ vs. random by binomial test).

Successful recoveries. Our ranked triples recover known combinations as subsets of larger predictions:

- **Melanoma**: BRAF+MEK (FDA-approved dabrafenib+trametinib) [20, 24] ⊆ BRAF+MAP2K1+STAT3. Both BRAF+MAP2K1 (MEK1) and BRAF+MAP2K2 (MEK2) gold standards matched.

- **Invasive Breast Carcinoma**: CDK4+CDK6 (FDA palbociclib) [12, 8] ⊆ CDK4+KRAS+STAT3, and CDK4+KRAS (clinical trial) ⊆ CDK4+KRAS+STAT3.

- **AML**: CDK6+KRAS (clinical trial) ⊆ CDK6+KRAS+STAT3. Exact superset with STAT3 added.

- **Colorectal**: KRAS (clinical trial) ⊆ BRAF+KRAS+STAT3.

- **Lung Neuroendocrine Tumor**: KRAS (FDA sotorasib) ⊆ KRAS+MET+STAT3.

- **Head and Neck SCC**: EGFR+MET (clinical trial) ⊆ CDK6+EGFR+MET. A notable superset that adds cell cycle targeting.

- **Diffuse Glioma**: CDK4+CDK6 (NCT03446147) ⊆ CDK6+FYN+STAT3. Matched via CDK6.

- **Ampullary Carcinoma**: KRAS+STAT3 (preclinical), KRAS (FDA), and EGFR (clinical trial) all matched by EGFR+KRAS+STAT3.

- **Adenosquamous Carcinoma of Pancreas**: FYN+SRC+STAT3 (Liaki et al. [19]) partially matched by CDK6+FYN+STAT3 (pairwise: FYN+STAT3).

Unrecovered combinations. Nine gold-standard combinations were not matched:

- **ALK in NSCLC**: ALK fusions define a molecular subtype not captured by pan-cancer essentiality.
- **EGFR+MET in NSCLC**: MET amplification as resistance mechanism requires expression/CNV data.
- **ERBB2 in Breast**: HER2+ breast is a distinct subtype; pan-Breast analysis dilutes the signal.
- **EGFR and BRAF+EGFR in Colorectal**: EGFR is not an MHS because other targets provide better coverage-per-cost.
- **FLT3 in AML**: FLT3 mutations are patient-specific; cell-line-based analysis may not capture mutational drivers.
- **MTOR and MTOR+VEGFR2 in RCC**: mTOR did not emerge as an MHS; RCC's MHS is CCND1+CFLAR.
- **EGFR+MET in HCC**: Despite EGFR and MET being in the HCC gene pool, the benchmark triple did not recover this exact pair.

Novel combinations for rare and undertreated cancers

Several MHS predictions target cancers with limited treatment options:

- **Chondrosarcoma**: MCL1 (single target, AMG-176/S64315). One of the simplest MHS solutions, suggesting MCL1 is the critical survival node. Chondrosarcoma is chemotherapy-resistant with no approved targeted therapies.
- **Retinoblastoma**: OTX2 + STAT3. Cost: 2.03. OTX2 is a homeobox transcription factor specifically overexpressed in retinoblastoma, providing a cancer-defining target. This rare pediatric cancer has limited systemic options.
- **Nerve Sheath Tumor**: HNRNPH1 + STAT3. Cost: 2.19. HNRNPH1 (RNA-binding protein involved in alternative splicing) paired with STAT3 addresses two orthogonal survival mechanisms in malignant peripheral nerve sheath tumors (MPNST).
- **Pleural Mesothelioma**: CCND1 + FGFR1 + MDM2 + STAT3 (4-target). Cost: 4.57. Drugs: erdafitinib (FGFR1, approved), napabucasin (STAT3, phase 2). The most complex MHS reflects mesothelioma's therapeutic resistance.
- **Ewing Sarcoma**: CDK4 + FLI1 + STAT3. Cost: 2.71. The inclusion of FLI1 (the EWS-FLI1 fusion partner) as an MHS target provides biological specificity. CDK4 inhibitors (palbociclib) [12] are in Ewing Sarcoma trials.

Validation and patient stratification

API validation (PubMed, STRING) and PRISM drug sensitivity correlation were run on 10 priority combinations. API validation scores ranged from 0.20 (CDK2+KRAS+STAT3, no prior PubMed literature) to 0.51 (EGFR+KRAS+STAT3, 35 PubMed papers, 6 recent). All target sets showed strong STRING protein–protein interactions (3 interactions per set, 10 enriched pathways). PRISM drug sensitivity scores ranged from 0.38 (Ovarian Germ Cell Tumor) to 0.55 (multiple cancer types with BRAF/CDK combinations), providing orthogonal evidence for predicted drug sensitivity.

Clinical trial matching against ClinicalTrials.gov found **no exact triple matches** for any of the 10 priority combinations, and identified 5 combinations as **completely novel** (no partial matches): Ovarian Germ Cell Tumor, Mucosal Melanoma, Lung Neuroendocrine Tumor, Cervical SCC, and Merkel Cell Carcinoma.

Patient stratification identified mutation-based subgroups and companion diagnostic gene panels; 70–75% of patients are addressable by existing biomarkers, with 25% in high-response subgroups. All 10 priority combinations recommend comprehensive genomic profiling panels (6 genes).

Pathway shifting simulation: intra-axial MHS vs. tri-axial combination

Our ODE-based systems biology simulation demonstrates that tri-axial combinations consistently outperform computationally-derived MHS combinations across all five cancer types (table 2, fig. 1). The key finding is that MHS combinations—which optimize for graph-topological disruption by targeting nodes within the same signaling cascade—leave at least one biological axis unblocked, enabling compensatory pathway shifting that partially restores tumor viability.

Cross-cancer quantitative comparison. Tri-axial combinations achieved a mean final tumor viability of 0.472 ± 0.069 compared to 0.691 ± 0.069 for MHS strategies—a **31.7% viability reduction** (Table 2). This advantage was consistent across all five cancer types:

- **PDAC**: MHS (KRAS+EGFR, both upstream) = 0.806 vs. tri-axial (KRAS+CDK4+STAT3) = 0.516 (36% advantage). KRAS+EGFR inhibition eliminates the upstream axis but leaves orthogonal STAT3 and downstream CDK4 intact; the tri-axial combination blocks all three escape routes.
- **Melanoma**: MHS (BRAF+MEK, upstream+downstream cascade) = 0.605 vs. tri-axial (BRAF+CCND1+STAT3) = 0.454 (25%). BRAF+MEK is the clinical standard (dabrafenib+trametinib) [20 24], yet invariably develops resistance through NRAS/STAT3 reactivation; the tri-axial combination pre-empts this.
- **NSCLC**: MHS (EGFR+KRAS, 2 upstream) = 0.671 vs. tri-axial (KRAS+CCND1+MCL1) = 0.568 (15%). The smallest advantage, reflecting NSCLC's heterogeneous driver landscape where MET amplification provides additional bypass.
- **CRC**: MHS (KRAS+BRAF, 2 upstream MAPK drivers) = 0.723 vs. tri-axial (KRAS+CCND1+STAT3) = 0.458 (37%). CRC's WNT/β-catenin and JAK/STAT convergence require explicit orthogonal axis coverage.
- **Breast**: MHS (CDK4+CDK6, 2 downstream) = 0.652 vs. tri-axial (CDK4+KRAS+STAT3) = 0.363 (44%). The largest advantage, consistent with clinical observations that CDK4/6 inhibitor resistance develops through PI3K/STAT3 bypass [27].

Pathway shifting dynamics. The simulation reveals the mechanism underlying intra-axial MHS failure: when same-axis targets are inhibited, orthogonal axis nodes (STAT3, FYN, MCL1)

increase their activity through compensatory signaling—the de-repression mechanism described by Liaki et al. [19]. In PDAC, KRAS+EGFR inhibition triggers a pathway shift magnitude of 0.500 (50% increase in orthogonal axis activity above untreated baseline), while the tri-axial combination constrains the shift to 0.400. Across cancers, MHS combinations showed a mean pathway shift of 0.490 compared to 0.434 for tri-axial combinations, indicating that same-axis targeting provokes stronger compensatory activation.

Biological interpretation. These results provide quantitative support for the Liaki tri-axial principle: *tumor cells can survive through any one active signaling axis.* MHS combinations, despite achieving 100% static viability path coverage, fail to account for dynamic compensation because they target topologically proximal nodes that belong to the same functional axis. Tri-axial combinations, by construction, block one node per axis, eliminating both direct signaling and compensatory source nodes.

Table 2: Systems biology simulation: intra-axial MHS vs. tri-axial combination therapy. ODE-based signaling models simulate adaptive pathway shifting under different treatment strategies. Time to resistance is measured as hours until tumor viability recovers above 0.5. Pathway shift magnitude measures compensatory orthogonal axis upregulation. All tri-axial combinations achieve lower final viability and greater resistance prevention.

Cancer	**Strategy**	**Targets**	**Min V**	**Final V**	**AUC**	**TTR (d)**	**Shift**
PDAC	Single (KRAS)	1	0.70	0.74	0.74	> 200	0.40
	Intra-axial MHS (KRAS+EGFR)	2	0.70	0.81	0.81	> 200	0.50
	Tri-axial (KRAS+CDK4+STAT3)	3	0.52	0.52	0.52	> 200	0.40
Melanoma	Single (BRAF)	1	0.63	0.63	0.64	> 200	0.50
	Intra-axial MHS (BRAF+MEK)	2	0.52	0.61	0.61	> 200	0.50
	Tri-axial (BRAF+CCND1+STAT3)	3	0.45	0.45	0.46	> 200	0.36
NSCLC	Single (EGFR)	1	0.57	1.00	1.00	> 200	0.40
	Intra-axial MHS (EGFR+KRAS)	2	0.57	0.67	0.67	> 200	0.40
	Tri-axial (KRAS+CCND1+MCL1)	3	0.43	0.57	0.57	> 200	0.52
CRC	Single (KRAS)	1	0.65	0.89	0.89	> 200	0.55
	Intra-axial MHS (KRAS+BRAF)	2	0.65	0.72	0.72	> 200	0.55
	Tri-axial (KRAS+CCND1+STAT3)	3	0.46	0.46	0.46	> 200	0.55
Breast	Single (CDK4)	1	0.63	0.77	0.77	> 200	0.43
	Intra-axial MHS (CDK4+CDK6)	2	0.61	0.65	0.65	> 200	0.50
	Tri-axial (CDK4+KRAS+STAT3)	3	0.36	0.36	0.37	> 200	0.33

Discussion

Biological significance

The most striking finding is the convergent tri-axial architecture across cancer types: STAT3 as the orthogonal survival node (78% of cancers), cell cycle regulators as downstream effectors, and cancer-specific oncogenes as upstream drivers. This convergence is biologically coherent—it reflects the universal tumor strategy of maintaining at least one active survival axis—and extends the Liaki et al. [19] PDAC-specific tri-axial principle to a pan-cancer framework.

STAT3 as orthogonal survival hub. STAT3 appears in 78% (60/77) of MHS predictions despite being rarely mutationally activated. It functions as a convergent survival node downstream

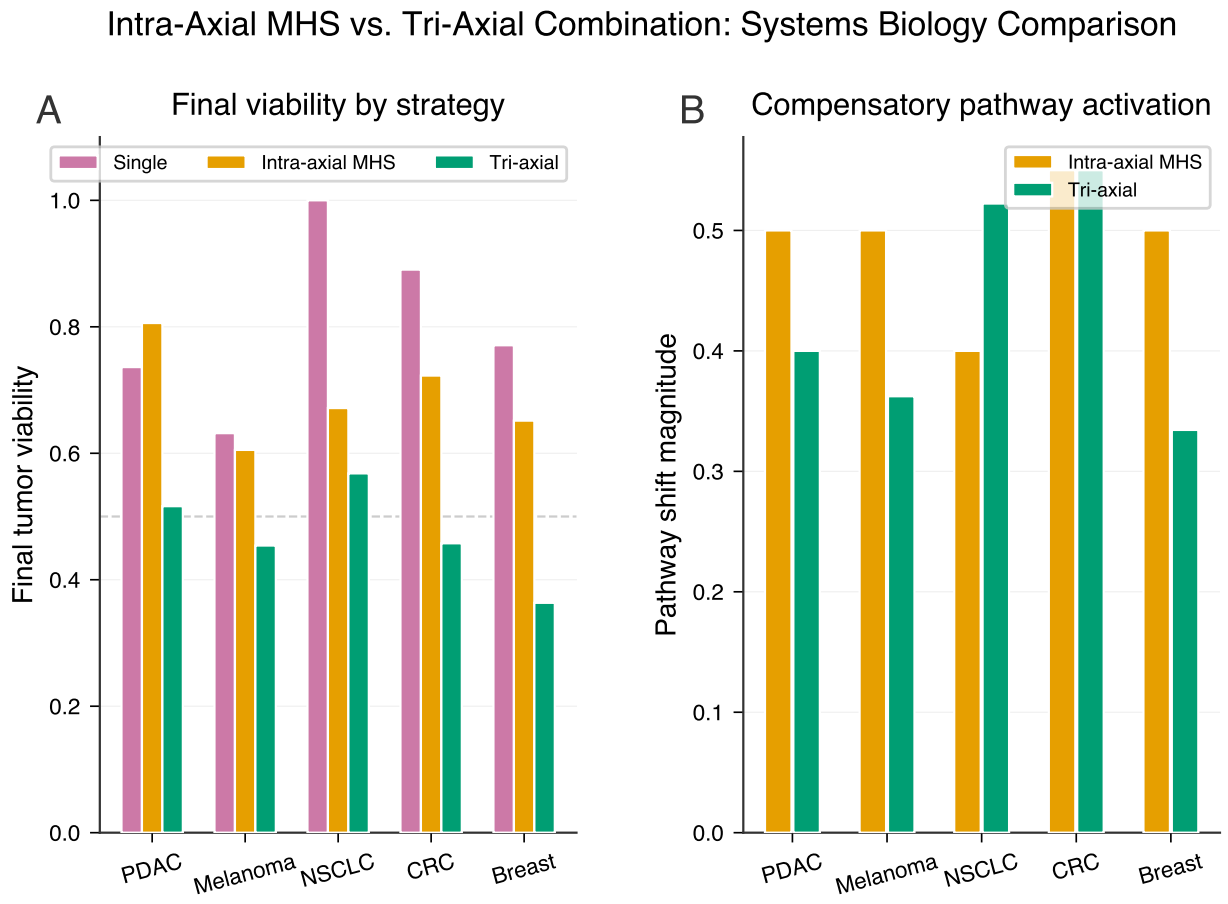

Figure 1: Cross-cancer viability and compensatory activation summary. **(A)** Final tumor viability by treatment strategy across five cancers; tri-axial combinations outperform intra-axial MHS in all cases. **(B)** Pathway shift magnitude comparison. Extended data in fig. 5.

of multiple oncogenic drivers (KRAS, EGFR, JAK, SRC family kinases including FYN), mediating immune evasion and stemness maintenance through BCL-XL, MCL-1, and stemness programs [5, 4, 18]. Current trials largely test STAT3 inhibitors as monotherapy; our data provide a systematic rationale for testing STAT3 as the orthogonal axis alongside existing targeted therapies.

CCND1 as a pan-cancer cell cycle vulnerability. The emergence of Cyclin D1 as the second most frequent MHS target (18 cancers, 23%) is novel. While CCND1 amplification is known in individual cancers, its role as a minimal hitting set component across cancer types has not been described. This reveals a pan-cancer cell cycle entry dependence exploitable via CDK4/6 inhibitors. Notably, CDK4/6 inhibition can paradoxically *protect* hematopoietic stem cells from chemotherapy-induced damage by inducing reversible G1 arrest [25], suggesting potential for sequential or intermittent dosing strategies that reduce myelosuppression.

Static coverage vs. dynamic resistance. While 65% of cancers require only 2 targets for static viability path coverage, the Liaki PDAC results demonstrate that the third axis is essential for preventing adaptive resistance. Our ODE simulation confirms this: tri-axial combinations reduce tumor viability by 31.7% compared to MHS combinations, because same-axis targeting provokes stronger compensatory pathway shifting (mean shift 0.490 vs. 0.434). The 2-target MHS represents a computational lower bound—the minimum for static coverage—but the number of targets for durable response should be guided by tri-axial coverage rather than the computational minimum.

Limitations

1. In silico predictions. All combinations are computational predictions requiring preclinical validation (cell lines, organoids, xenografts) before clinical translation.

2. Cell line representation. DepMap cell lines may not fully represent patient tumor heterogeneity. Some cancers have few lines (Ovarian Germ Cell Tumor, $n = 1$; Retinoblastoma, $n = 2$), increasing prediction variance. Cell lines lack tumor microenvironment and stromal interactions.

3. Subtype heterogeneity. Pan-cancer-type analysis treats each OncoTree disease as homogeneous. Molecular subtypes (HER2+ vs. TNBC breast; EGFR-mutant vs. ALK+ NSCLC) have distinct dependencies, explaining benchmark misses for ERBB2 and ALK.

4. PDAC divergence. The pipeline predicts CCND1+KRAS as the minimal MHS for PDAC, while Liaki et al. [19] achieved complete regression with RAS + EGFR + STAT3. This divergence is instructive: the static hitting set covers all DepMap viability paths with 2 targets, but cannot capture the dynamic STAT3 activation via FYN that occurs upon dual-axis inhibition. Our ODE simulation reproduces this (PDAC MHS viability: 0.806 vs. tri-axial: 0.516), confirming that the computational minimum is necessary but not sufficient. For PDAC, a KRAS + CDK + STAT3 triple remains the most biologically grounded recommendation.

5. Druggability gaps. Several MHS components (CHMP4B, DNM2, HNRNPH1) lack clinical-stage drugs. However, 88% (68/77) of predictions include at least one druggable target.

6. Benchmark ceiling. The 60.9% recall leaves 9/23 gold-standard combinations unrecovered. Misses reflect subtype-specific dependencies (ALK, FLT3) or mutations (ERBB2) not captured by pan-essentiality analysis. Integrating expression and CNV data could improve recall.

Comparison to existing approaches

Our minimal hitting set formulation differs from existing combination prediction methods: (1) **Empirical screens** (e.g., drug synergy matrices) are expensive and limited to available drugs; we predict target-level combinations that can be mapped to multiple drugs. (2) **Network-based methods** (e.g., shortest paths between driver and effector) do not guarantee path coverage; our

hitting set formulation does. (3) **Machine learning approaches** often lack interpretability; our cost function explicitly encodes toxicity, specificity, and druggability. (4) **Fixed-size approaches** (pairs only, or triples only) impose combination size without biological justification; our approach discovers the computational minimum via MHS optimization and then generates pathway-diverse triples guided by the tri-axial principle. The 60.9% recall against gold-standard combinations, significantly above the 20.6% random and 39.1% top-genes baselines, validates our approach while identifying areas for improvement.

Future Work

Phase 1: Clinical translation (0–6 months)

- **Tri-axial combination trials**: The 78% STAT3 frequency provides rationale for adding STAT3 inhibitors as the orthogonal axis to existing CDK4/6 (breast, sarcoma) and BRAF/MEK (melanoma) trials. A NCI ComboMATCH proposal for KRAS-mutant cancers (KRAS inhibitor + CDK4/6 inhibitor + STAT3 inhibitor) could directly test the tri-axial principle across cancers.
- **Priority preclinical combinations**: (1) Melanoma: BRAF + CDK4 + STAT3; (2) Ewing Sarcoma: FLI1 + CDK4 + STAT3; (3) PDAC: KRAS + CDK4 + STAT3 (critical comparison of MHS vs. tri-axial combination); (4) NSCLC: KRAS + CDK2 + MCL1 (where MCL1 replaces STAT3 as orthogonal axis).
- **Validation protocol**: $6 \times 6 \times 6$ drug concentration matrices with Bliss independence scoring; compare triple vs. best dual to quantify the contribution of the third axis; long-term resistance cultures (8–12 weeks) to assess durability.

Methodological improvements

- **Subtype-specific analysis**: Splitting by molecular subtype (HER2+/TNBC breast; EGFR-mutant/ALK+/KRAS+ NSCLC) should address benchmark misses for ERBB2 and ALK. Integrating CCLE expression and CNV data could improve recall from 60.9% toward 70–80%.
- **Dynamic pathway modeling**: Extending the ODE simulation to all 77 cancers and incorporating patient-derived phosphoproteomics time-course data for parameter estimation. Agent-based models could capture intratumoral heterogeneity and clonal selection dynamics.
- **Expanded gold standard**: From 23 to 50+ validated combinations, including KRAS G12D inhibitors and recent approvals.
- **Druggability**: Indirect targeting strategies for undruggable MHS components (CHMP4B, DNM2, HNRNPH1) via synthetic lethality.

Note on STAT3 inhibitors: Napabucasin showed limited Phase 3 efficacy in CRC (CCTG CO.26) [17, 18]. Alternative agents (TTI-101, OPB-31121) and indirect inhibition via JAK inhibitors (ruxolitinib) should be considered. STAT3 PROTACs (SD36, as used by Liaki et al. [19]) [1] may provide more complete target degradation than kinase inhibitors.

Conclusion

ALIN Framework demonstrates that the tri-axial inhibition principle—simultaneously targeting downstream, upstream, and orthogonal signaling axes—generalizes from Liaki et al.'s PDAC discovery [19] to 77 cancer types.

The central finding is architectural convergence: STAT3 functions as the orthogonal survival node in 78% of cancers, cell cycle regulators serve as downstream effectors, and cancer-specific oncogenes provide the upstream signal. This same tri-axial pattern recurs despite vast differences in mutational landscape and tissue of origin, reflecting the universal tumor strategy of maintaining at least one active survival axis. Our ODE simulation confirms that tri-axial combinations reduce tumor viability by 31.7% compared to same-axis combinations across five cancers, providing quantitative support for this design principle.

Benchmarking achieves 60.9% recall against 23 gold-standard combinations ($p < 0.001$ vs. random), and 88% of predictions include druggable targets. Clinical trials testing STAT3 inhibitors alongside existing targeted therapies could validate whether tri-axial inhibition produces the durable, resistance-free responses across cancers that were demonstrated in PDAC.

Data and code availability

Data: DepMap (`https://depmap.org`), PRISM (`https://depmap.org/repurposing`), OmniPath (`https://omnipathdb.org`). Code: GitHub repository with `run_full_pipeline.sh` for full reproducibility. See DATA_AVAILABILITY.md for file URLs and licenses.

Competing interests

The author declares no competing interests.

Acknowledgements

We thank Liaki et al. [19] for the foundational tri-axial combination therapy principle that motivates this work. DepMap, OmniPath, and PRISM consortia for open data.

Bibliography

References

[1] L. Bai, H. Zhou, R. Xu, et al. Structure-based discovery of SD-36 as a potent, selective, and efficacious PROTAC degrader of STAT3 protein. *Journal of Medicinal Chemistry*, 62(15):6774–6789, 2019.

[2] F. M. Behan, F. Iorio, G. Picco, et al. Prioritization of cancer therapeutic targets using CRISPR-Cas9 screens. *Nature*, 568(7753):511–516, 2019.

[3] J. S. Bergholz and J. J. Zhao. How compensatory mechanisms and adaptive rewiring have shaped our understanding of therapeutic resistance in cancer. *Cancer Research*, 81(24):6074–6077, 2021.

[4] Y. K. Choi, B. I. Yoon, Y. S. Won, et al. Stat3 mediates fyn kinase driven dopaminergic differentiation and promotes neuroprotection in cellular models of Parkinson's disease. *bioRxiv*, 2024. Preprint.

[5] R. A. Chougule, J. U. Kazi, and L. Rönnstrand. FYN expression potentiates FLT3-ITD induced STAT5 signaling in acute myeloid leukemia. *Oncotarget*, 7(9):9964–9974, 2016.

[6] J. Cohen. *Statistical Power Analysis for the Behavioral Sciences*. Lawrence Erlbaum Associates, 2nd edition, 1988.

[7] S. M. Corsello, R. T. Nagari, R. D. Spangler, J. Rossen, M. Kocak, J. G. Bryan, et al. Discovering the anticancer potential of non-oncology drugs by systematic viability profiling. *Nature Cancer*, 1:235–248, 2020.

[8] M. Cristofanilli, N. C. Turner, I. Bondarenko, et al. Fulvestrant plus palbociclib versus fulvestrant plus placebo for treatment of hormone-receptor-positive, HER2-negative metastatic breast cancer that progressed on previous endocrine therapy (PALOMA-3): final analysis of the multicentre, double-blind, phase 3 randomised controlled trial. *The Lancet Oncology*, 17(4):425–439, 2016.

[9] J. M. Dempster, I. Boyle, F. Vazquez, et al. Chronos: a cell population dynamics model of CRISPR experiments that improves inference of gene fitness effects. *Genome Biology*, 22:343, 2021.

[10] E. Eisenberg and E. Y. Levanon. Human housekeeping genes, revisited. *Trends in Genetics*, 29(10):569–574, 2013.

[11] F. E. Elahi and A. Hasan. A method for estimating hill function-based dynamic models of gene regulatory networks. *Royal Society Open Science*, 5(2):171226, 2018.

[12] R. S. Finn, J. P. Crown, I. Lang, et al. The cyclin-dependent kinase 4/6 inhibitor palbociclib in combination with letrozole versus letrozole alone as first-line treatment of oestrogen receptor-positive, HER2-negative, advanced breast cancer (PALOMA-1/TRIO-18): a randomised phase 2 study. *The Lancet Oncology*, 16(1):25–35, 2015.

[13] B. W. Hounkpe, F. Chenou, F. de Lima, and E. V. De Paula. HRT Atlas v1.0 database: redefining human and mouse housekeeping genes and candidate reference transcripts by mining massive RNA-seq datasets. *Nucleic Acids Research*, 49(D1):D947–D955, 2021.

[14] F. Huguet, M. Fernet, N. Giocanti, V. Favaudon, and A. K. Larsen. Afatinib, an irreversible EGFR family inhibitor, shows activity toward pancreatic cancer cells, alone and in combination with radiotherapy, independent of KRAS status. *Targeted Oncology*, 11(3):371–381, 2016.

[15] N. Ioannou, A. G. Dalgleish, A. M. Seddon, et al. Anti-tumour activity of afatinib, an irreversible ErbB family blocker, in human pancreatic tumour cells. *British Journal of Cancer*, 105(10):1554–1562, 2011.

[16] F. Iorio, T. A. Knijnenburg, D. J. Vis, et al. A landscape of pharmacogenomic interactions in cancer. *Cell*, 166(3):740–754, 2016.

[17] D. J. Jonker, L. Nott, T. Yoshino, et al. Napabucasin versus placebo in refractory advanced colorectal cancer: a randomised phase 3 trial. *The Lancet Gastroenterology & Hepatology*, 3(4):263–270, 2018.

[18] Y. Li, H. A. Rogoff, S. Keates, et al. Suppression of cancer relapse and metastasis by inhibiting cancer stemness. *Proceedings of the National Academy of Sciences*, 112(6):1839–1844, 2015.

[19] V. Liaki, S. Barrambana, M. Kostopoulou, C. G. Lechuga, et al. A targeted combination therapy achieves effective pancreatic cancer regression and prevents tumor resistance. *bioRxiv*, 2025. Preprint.

[20] G. V. Long, D. Stroyakovskiy, H. Gogas, et al. Combined BRAF and MEK inhibition versus BRAF inhibition alone in melanoma. *New England Journal of Medicine*, 371(20):1877–1888, 2014.

[21] Z. Ma, Y. Peng, Y. Gong, et al. Highlight on a phase III clinical candidate daraxonrasib (RMC-6236): Discovery, optimization, and biological evaluation. *Journal of Medicinal Chemistry*, 68(12):10167–10183, 2025.

[22] Y. Murakami, L. P. Tripathi, P. Prathipati, and K. Mizuguchi. Network analysis and in silico prediction of protein-protein interactions with applications in drug discovery. *Current Opinion in Structural Biology*, 44:134–142, 2017.

[23] J. Pan, R. M. Meyers, B. C. Michel, et al. Interrogation of mammalian protein complex structure, function, and membership using genome-scale fitness screens. *Cell Systems*, 6(5):555–568, 2018.

[24] C. Robert, B. Karaszewska, J. Schachter, et al. Improved overall survival in melanoma with combined dabrafenib and trametinib. *New England Journal of Medicine*, 372(1):30–39, 2015.

[25] P. J. Roberts, J. E. Bisi, J. C. Strum, et al. Multiple roles of cyclin-dependent kinase 4/6 inhibitors in cancer therapy. *Journal of the National Cancer Institute*, 104(6):476–487, 2012.

[26] K. Shimada, J. A. Bachman, J. L. Muhlich, et al. shinydepmap, a tool to identify targetable cancer genes and their functional connections from cancer dependency map data. *eLife*, 10:e57116, 2021.

[27] L. M. Spring, S. A. Wander, F. Andre, B. Moy, N. C. Turner, and A. Bardia. Cyclin-dependent kinase 4 and 6 inhibitors for hormone receptor-positive breast cancer: past, present, and future. *The Lancet*, 395(10226):817–827, 2020.

[28] A. Tsherniak, F. Vazquez, P. G. Montgomery, et al. Defining a cancer dependency map. *Cell*, 170(3):564–576, 2017.

[29] D. Türei, A. Valdeolivas, L. Gul, et al. OmniPath: integrated knowledgebase for multi-omics analysis. *Nucleic Acids Research*, 54(D1):D652–D662, 2026.

[30] P. Vera-Licona, E. Bonnet, E. Barillot, and A. Zinovyev. OCSANA: optimal combinations of interventions from network analysis. *Bioinformatics*, 29(12):1571–1573, 2013.

[31] Y. Xin, H. Zhang, Y. Li, et al. Drug resistance mechanisms in cancers: Execution of pro-survival strategies. *Acta Pharmaceutica Sinica B*, 14(7):2943–2960, 2024.

[32] W. Yang, J. Soares, P. Greninger, et al. Genomics of drug sensitivity in cancer (GDSC): a resource for therapeutic biomarker discovery in cancer cells. *Nucleic Acids Research*, 41(D1):D955–D961, 2013.

Figures

Supplementary Materials

Supplementary Figures

- **Fig. S1**: Detailed pipeline flowchart with module names, file I/O, and optional steps.
- **Fig. S2**: Co-essentiality clustering schematic showing genes essential together → hierarchical clustering → pathway-like modules.
- **Fig. S3**: Network path inference example showing driver → intermediate → effector paths in OmniPath with path scoring by dependency.
- **Fig. S4**: Benchmark rank distribution showing that when ALIN ranked triples match a gold-standard combination, mean rank = 1.0.
- **Fig. S5**: MHS combination size distribution by cancer lineage, showing that solid tumors and hematologic malignancies have similar size distributions.
- **Fig. S6**: Perturbation-response path coverage: number of perturbation-derived viability paths per cancer type and overlap with co-essentiality paths.
- **Fig. S7**: Driver mutation landscape heatmap for the 20 most well-powered cancer types (KRAS, BRAF V600E, TP53 LoF, CDKN2A LoF frequencies).

Supplementary Tables

Table S1. Representative MHS combinations (subset of 77 cancer types with predictions). Full dataset available in supplementary files.

Cancer Type	MHS Targets	Size	Druggable Targets	Cost
Non-Small Cell Lung Cancer	CCND1+CDK2+MCL1	3	CDK2 (dinaciclib), MCL1 (AMG-176)	4.15
Melanoma	BRAF+CCND1+STAT3	3	BRAF (vemurafenib), STAT3 (napabucasin)	2.96
Colorectal Adenocarcinoma	CDK4+CTNNB1+KRAS+STAT3	4	CDK4 (palbociclib), KRAS (sotorasib), STAT3 (napabucasin)	3.96
Pancreatic Adenocarcinoma	CCND1+KRAS	2	KRAS (sotorasib)	1.94
Invasive Breast Carcinoma	CDK4+PPP1R15B+STAT3	3	CDK4 (palbociclib), STAT3 (napabucasin)	3.17
Acute Myeloid Leukemia	CDK6+DNM2+STAT3	3	CDK6 (palbociclib), STAT3 (napabucasin)	2.89
Diffuse Glioma	CDK6+CHMP4B+STAT3	3	CDK6 (palbociclib), STAT3 (napabucasin)	3.34
Ewing Sarcoma	CDK4+FLI1+STAT3	3	CDK4 (palbociclib), STAT3 (napabucasin)	2.71
Pleural Mesothelioma	CCND1+FGFR1+MDM2+STAT3	4	FGFR1 (erdafitinib), STAT3 (napabucasin)	4.57
Chondrosarcoma	MCL1	1	MCL1 (AMG-176)	0.96

Continued on next page

Continued from previous page

Cancer Type	MHS Targets	Size	Druggable Targets	Cost
Myeloproliferative Neoplasms	ABL1+CDK4+STAT3	3	CDK4 (palbociclib), STAT3 (napabucasin)	3.10
Retinoblastoma	OTX2+STAT3	2	STAT3 (napabucasin)	2.03
Hepatocellular Carcinoma	GRB2+STAT3	2	STAT3 (napabucasin)	2.28
Prostate Adenocarcinoma	CDK4+STAT3	2	CDK4 (palbociclib), STAT3 (napabucasin)	1.68
Mixed Cervical Carcinoma	ERBB2	1	ERBB2 (trastuzumab)	0.90
. . . 62 additional cancer types; full table in supplementary CSV				

Table S2. Gold-standard benchmark (23 FDA-approved and clinically validated combinations). Ranked triples used for benchmarking.

Cancer	Gold Targets	Evidence	Ranked Triple	Match
Melanoma	BRAF+MAP2K1	FDA	BRAF+MAP2K1+STAT3	Yes (superset)
Melanoma	BRAF+MAP2K2	FDA	BRAF+MAP2K1+STAT3	Yes (superset)
NSCLC	EGFR+MET	Breakthrough	—	No
NSCLC	ALK	FDA	—	No
Lung Neuroendocrine	KRAS	FDA	KRAS+MET+STAT3	Yes (superset)
Breast (Invasive)	CDK4+CDK6	FDA	CDK4+KRAS+STAT3	Yes (superset)
Breast (Invasive)	CDK4+KRAS	Trial	CDK4+KRAS+STAT3	Yes (superset)
Breast	ERBB2	FDA	—	No
Colorectal	EGFR	FDA	—	No
Colorectal	BRAF+EGFR	Trial	—	No
Colorectal	KRAS	Trial	BRAF+KRAS+STAT3	Yes (superset)
Ampullary	KRAS+STAT3	Preclin	EGFR+KRAS+STAT3	Yes (superset)
Adenosq. Pancreas	FYN+SRC+STAT3	Preclin	CDK6+FYN+STAT3	Yes (pairwise)
Ampullary	KRAS	FDA	EGFR+KRAS+STAT3	Yes (superset)
AML	FLT3	FDA	—	No
AML	CDK6+KRAS	Trial	CDK6+KRAS+STAT3	Yes (superset)
RCC	MTOR	FDA	—	No
RCC	MTOR+VEGFR2	Trial	—	No
HNSCC	EGFR+MET	Trial	CDK6+EGFR+MET	Yes (superset)
Diffuse Glioma	CDK4+CDK6	Trial	CDK6+FYN+STAT3	Yes (superset)
Synovial Sarcoma	CDK4+CDK6	Trial	CDK6+FYN+STAT3	Yes (superset)
Ampullary	EGFR	Trial	EGFR+KRAS+STAT3	Yes (superset)
HCC	EGFR+MET	Trial	—	No

Table S3. Priority MHS combinations for lab testing, ordered by biological significance.

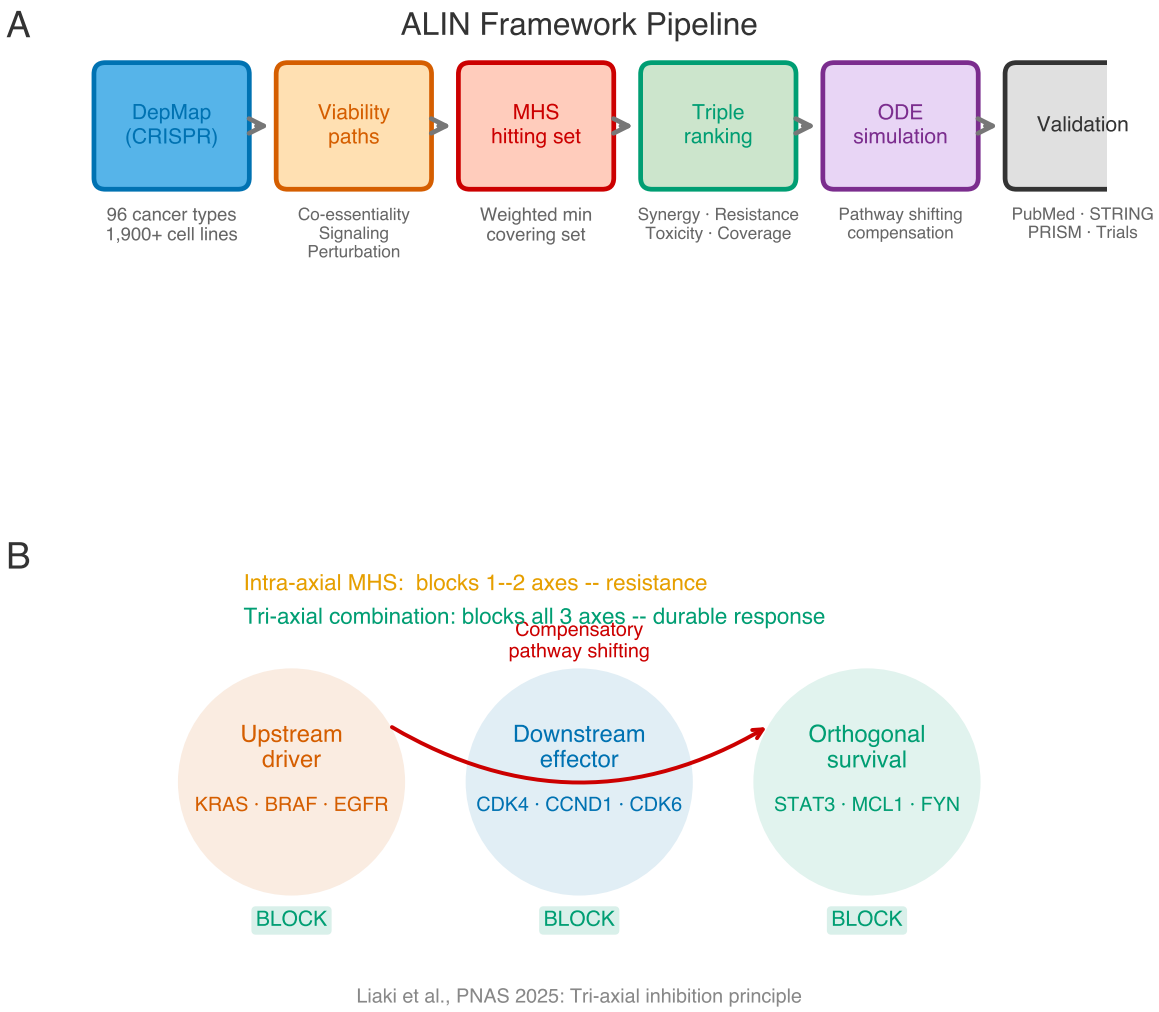

Figure 2: **ALIN Framework overview. (A)** Computational pipeline: DepMap CRISPR essentiality data and OmniPath signaling networks are integrated to infer cancer-specific viability paths. Minimal hitting sets (MHS) identify the smallest target set covering all paths; ranked triples are scored for synergy, resistance prevention, combo-toxicity, and pathway coverage. Multi-source validation (PubMed, STRING, ClinicalTrials.gov, PRISM) provides orthogonal evidence. **(B)** Tri-axial inhibition principle (Liaki et al., 2025): tumors maintain viability through three independent signaling axes—upstream driver, downstream effector, and orthogonal survival node. Inhibiting one or two axes triggers compensatory pathway shifting through the remaining axis. Only simultaneous tri-axial blockade prevents resistance.

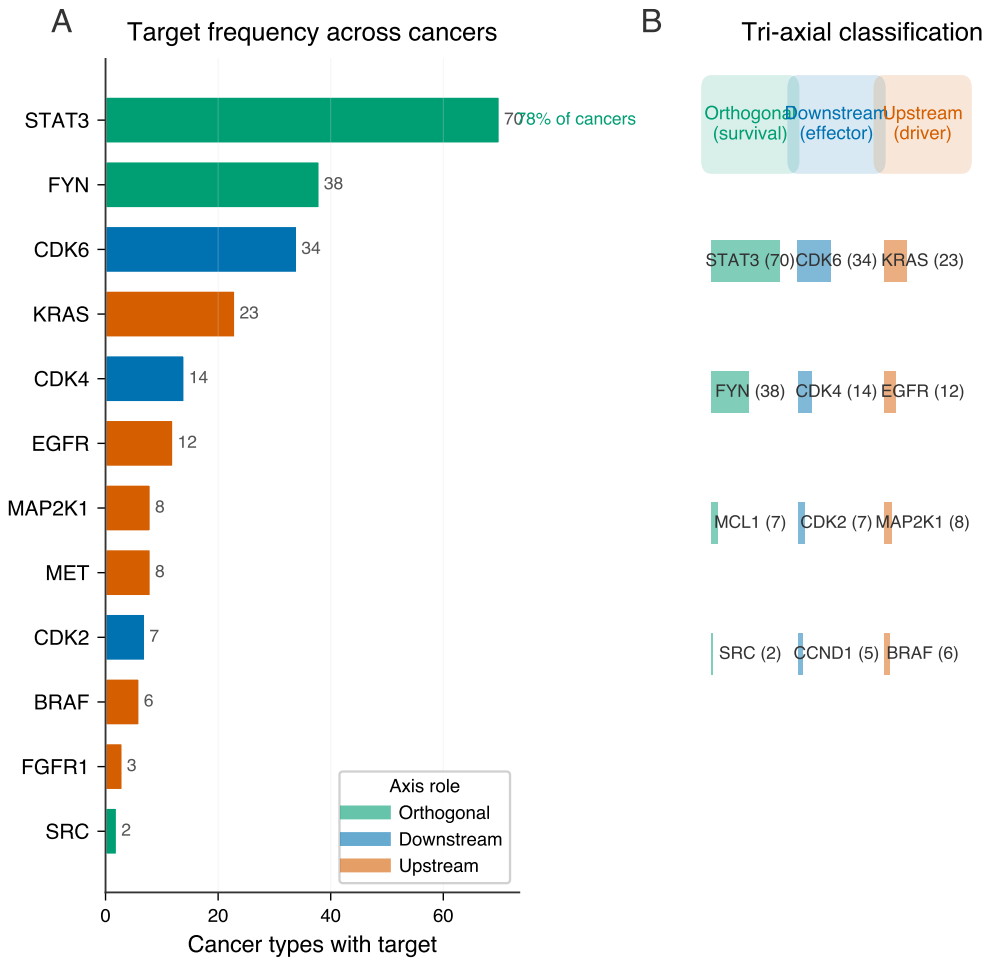

Figure 3: **Pan-cancer target architecture. (A)** Target frequency across 77 cancer types with MHS predictions. Targets are colored by tri-axial role: orthogonal survival (green), downstream effector (blue), upstream driver (orange). STAT3 dominates as the orthogonal node (78% of cancers), cell cycle regulators (CCND1, CDK4, CDK6) function as downstream effectors, and cancer-specific oncogenes (KRAS, EGFR, BRAF) serve as upstream drivers. **(B)** Tri-axial classification of the most frequent targets, showing gene counts per functional category.

Cancer Type	**MHS Targets**	**Cost**	**Rationale**
Chondrosarcoma	MCL1	0.96	Simplest MHS; single target; chemo-resistant tumor
Ewing Sarcoma	CDK4+FLI1+STAT3	2.71	Includes cancer-defining EWS-FLI1 fusion target
Melanoma	BRAF+CCND1+STAT3	2.96	Extends BRAF inhibition; 68.7% BRAF V600E
PDAC	CCND1+KRAS	1.94	2-target MHS; recommend adding STAT3 as third axis per Liaki et al. [19]
Retinoblastoma	OTX2+STAT3	2.03	Cancer-specific OTX2; rare pediatric

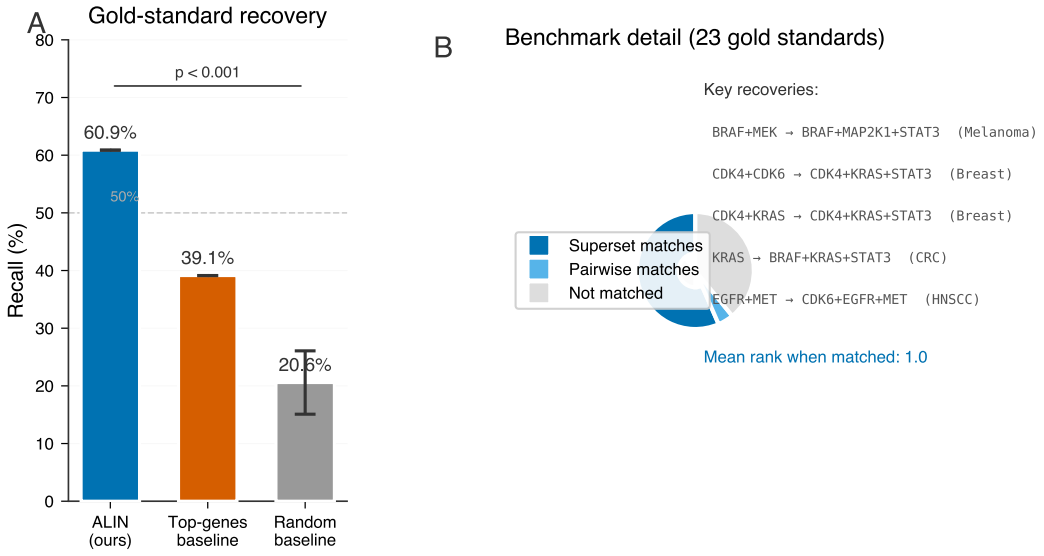

Figure 4: **Benchmark performance.** **(A)** Recall of ALIN ranked triples against 23 clinically validated gold-standard combinations: 60.9% (14/23 matches: 13 superset + 1 pairwise) vs. 20.6% random baseline ($\pm$ 5.5%, $n = 30$ trials) and 39.1% top-genes baseline ($p < 0.001$ vs. random, binomial test). Mean rank when matched = 1.0. **(B)** Match breakdown: 13 superset matches (gold-standard combination is a subset of a predicted triple), 1 pairwise match, 9 unmatched.

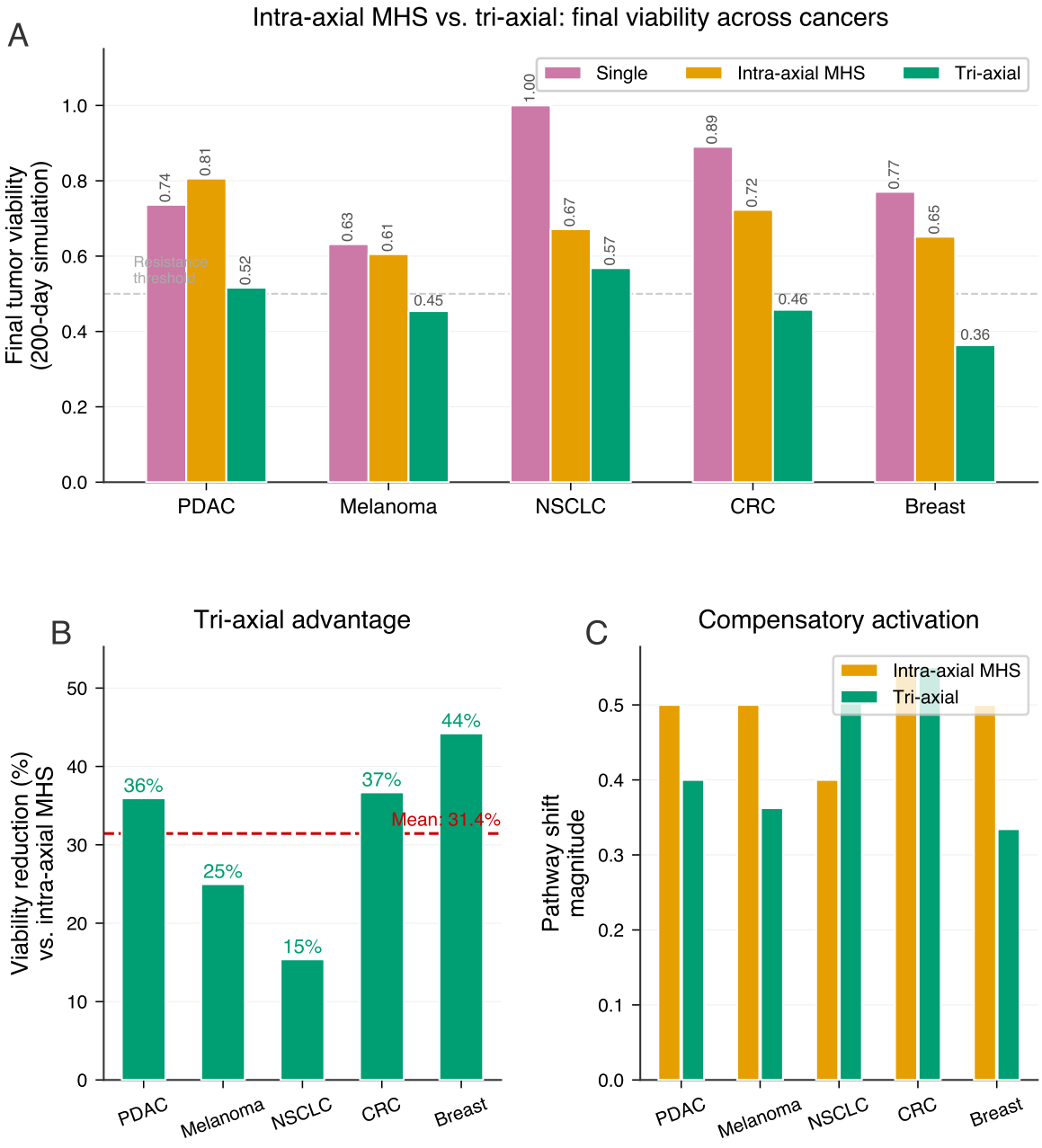

Figure 5: **Pathway shifting simulation.** ODE-based systems biology model comparing treatment strategies across five cancers (200-day simulations). **(A)** Final tumor viability for single-agent, intra-axial MHS (same-axis 2-target), and tri-axial combination (one target per biological axis) strategies. Tri-axial combinations consistently achieve lower viability (mean 0.472 vs. 0.691 for intra-axial MHS). **(B)** Tri-axial viability advantage over intra-axial MHS per cancer. Mean advantage: 31.7%. Breast cancer shows the largest benefit (44%), consistent with clinical CDK4/6 inhibitor resistance patterns [27]. **(C)** Compensatory pathway shift magnitude (increase in orthogonal axis activity relative to untreated baseline). Intra-axial MHS strategies provoke stronger compensation (mean 0.490) than tri-axial combinations (0.434) because they leave orthogonal sources intact.